



1 **Development of Korean Air Quality Prediction System**
2 **version 1 (KAQPS v1): an operational air quality**
3 **prediction system with focuses on practical issues**

4
5 **Kyunghwa Lee^{1,2}, Jinhyeok Yu², Sojin Lee³, Mieun Park^{4,5}, Hun Hong², Soon Young**
6 **Park², Myungje Choi⁶, Jhoon Kim⁶, Younha Kim⁷, Jung-Hun Woo⁷, Sang-Woo Kim⁸**
7 **and Chul H. Song^{2*}**

8

- 9 1. Environmental Satellite Center, Climate and Air Quality Research Department, National
10 Institute of Environmental Research (NIER), Incheon, Republic of Korea
11 2. School of Earth Sciences and Environmental Engineering, Gwangju Institute of Science
12 and Technology (GIST), Gwangju, Republic of Korea
13 3. Department of Earth and Atmospheric Sciences, University of Houston, Texas, USA
14 4. Air Quality Forecasting Center, Climate and Air Quality Research Department, National
15 Institute of Environmental Research (NIER), Incheon, Republic of Korea
16 5. Environmental Meteorology Research Division, National Institute of Meteorological
17 Sciences (NIMS), Jeju, Republic of Korea
18 6. Department of Atmospheric Sciences, Yonsei University, Seoul, Republic of Korea
19 7. Department of Advanced Technology Fusion, Konkuk University, Seoul, Republic of
20 Korea
21 8. School of Earth and Environmental Sciences, Seoul National University, Seoul, Republic
22 of Korea

23

24

25 **Short title:** Operational air quality prediction system in Korea

26

27 **Corresponding author:** Chul H. Song (chsong@gist.ac.kr)

28



29 **Abstract**

30 For the purpose of providing reliable and robust air quality predictions, an
31 operational air quality prediction system was developed for the main air quality criteria
32 species in South Korea (PM_{10} , $PM_{2.5}$, CO, O_3 , and SO_2). The main caveat of the system is to
33 prepare the initial conditions (ICs) of the Community Multi-scale Air Quality (CMAQ)
34 model simulations using observations from the Geostationary Ocean Color Imager (GOCI)
35 and ground-based monitoring networks in northeast Asia. The performance of the air quality
36 prediction system was evaluated during the Korea-United States Air Quality Study (KORUS-
37 AQ) campaign period (1 May–12 June 2016). Data assimilation (DA) of optimal
38 interpolation (OI) with Kalman filter was used in this study. One major advantage of the
39 system is that it can predict not only particulate matter (PM) concentrations but also PM
40 chemical composition including five main constituents: sulfate (SO_4^{2-}), nitrate (NO_3^-),
41 ammonium (NH_4^+), organic aerosols (OAs), and elemental carbon (EC). In addition, it is also
42 capable of predicting the concentrations of gaseous pollutants (CO, O_3 and SO_2). In this sense,
43 this new operational air quality prediction system is comprehensive. The results with the ICs
44 (DA RUN) were compared with those of the CMAQ simulations without ICs (BASE RUN).
45 For almost all of the species, the application of ICs led to improved performance in terms of
46 correlation, errors, and biases over the entire campaign period. The DA RUN agreed
47 reasonably well with the observations for PM_{10} (IOA = 0.60; MB = -13.54) and $PM_{2.5}$ (IOA =
48 0.71; MB = -2.43) as compared to the BASE RUN for PM_{10} (IOA = 0.51; MB = -27.18) and
49 $PM_{2.5}$ (IOA = 0.67; MB = -9.9). A significant improvement was also found with the DA RUN
50 in terms of bias. For example, for CO, the MB of -0.27 (BASE RUN) was greatly enhanced
51 to -0.036 (DA RUN). In the cases of O_3 and SO_2 , the DA RUN also showed better



52 performance than the BASE RUN. Further, several more practical issues frequently
53 encountered in the operational air quality prediction system were also discussed. In order to
54 attain more accurate ozone predictions, the DA of NO₂ mixing ratios should be implemented
55 with careful consideration of the measurement artifacts (i.e., inclusion of alkyl nitrates, HNO₃,
56 and PANs in the ground-observed NO₂ mixing ratios). It was also discussed that, in order to
57 ensure accurate nocturnal predictions of the concentrations of the ambient species, accurate
58 predictions of the mixing layer heights (MLH) should be achieved from the meteorological
59 modeling. Several advantages of the current air quality prediction system, such as its non-
60 static free parameter scheme, dust episode prediction, and possible multiple implementations
61 of DA prior to actual predictions, were also discussed. These configurations are all possible
62 because the current DA system is not computationally expensive. In the ongoing and future
63 works, more advanced DA techniques such as the three-dimensional variational (3DVAR)
64 method and ensemble Kalman filter (EnK) are being tested and will be introduced to the
65 Korean operational air quality forecasting system.

66

67 **Keywords:** Air quality prediction; Particulate matter (PM); Geostationary satellite sensor
68 (GOCI); Air Korea; Data assimilation (DA); Dust episode predictions; NO₂ measurement
69 artifacts



70 **1. Introduction**

71 Air quality has long been considered an important issue in climate change, visibility,
72 and public health, and it is strongly dependent upon meteorological conditions, emissions,
73 and the transport of air pollutants. Air pollutants typically consist of atmospheric particles and
74 gases such as particulate matter (PM), carbon monoxide (CO), ozone (O₃), nitrogen dioxide
75 (NO₂), and sulfur dioxide (SO₂). These aerosols and gases play important roles in
76 anthropogenic climate forcing both directly (Bellouin et al., 2005; Carmichael et al., 2009;
77 IPCC, 2013; Scott et al., 2014) and indirectly (Bréon et al., 2002; IPCC, 2013; Penner et al.,
78 2004; Scott et al., 2014) in influencing the global radiation budget. Among the various air
79 pollutants, PM and surface O₃ are the most notorious health threats, as has been stated by
80 several previous studies (e.g. Carmichael et al., 2009; Dehghani et al., 2017; Khaniabadi et al.,
81 2017).

82 With the stated importance of atmospheric aerosols and gases, considerable research
83 efforts have been made to monitor and quantify their amounts in the atmosphere through
84 satellite-, airborne-, and ground-based observations as well as chemistry-transport model
85 (CTM) simulations. In South Korea, the Korean Ministry of the Environment (KMoE)
86 provides real-time chemical concentrations as measured by ground-based observations for six
87 criteria air pollutants (PM₁₀, PM_{2.5}, O₃, CO, SO₂, and NO₂) at the Air Korea website
88 (<https://www.airkorea.or.kr>). In addition, the National Institute of Environmental Research
89 (NIER) of South Korea provides air quality (chemical weather) predictions using multiple
90 CTM simulations. Air quality predictions are another crucial element for protecting public
91 health through the forecasting of high air pollution episodes in advance and alerting citizens
92 about these high episodes. In this context, reliable and robust chemical weather forecasts are



93 necessary to avoid any confusion caused by poor predictions given by CTM simulations.

94 Although there are various datasets representing air quality, limitations remain in the
95 observations and model outputs. Specifically, observation data are, in general, known to be
96 more accurate than model outputs, but they have spatial and temporal limitations. Unlike
97 observation data, models can provide meteorological and chemical information without any
98 spatial and temporal data discontinuity, but they do have an issue of inaccuracy. The major
99 causes of uncertainty in the results of CTM simulations are introduced from imperfect
100 emissions, meteorological fields, initial conditions (ICs), and physical and chemical
101 parameterizations in the models (Carmichael et al., 2008). In order to minimize the
102 limitations and maximize the advantages of observation data and model outputs, there have
103 been numerous attempts to provide accurate and spatially- as well as temporally- continuous
104 information on chemical composition in the atmosphere by integrating observation data with
105 model outputs via data assimilation (DA) techniques.

106 Although the Korean operational numerical weather prediction (NWP) carried out by
107 the Korea Meteorological Administration (KMA) employs various DA techniques, almost no
108 previous efforts have been made to develop a chemical weather prediction system with DA in
109 South Korea. Therefore, in the present study, an operational chemical weather prediction
110 system named as Korean Air Quality Prediction System version 1 (KAQPS v1) was
111 developed by preparing ICs via DA for the Community Multi-scale Air Quality (CMAQ)
112 model (Byun and Schere, 2006; Byun and Ching, 1999) using satellite- and ground-based
113 observations for particulate matter (PM) and atmospheric gases such as CO, O₃, and SO₂. The
114 performances of the system were then demonstrated during the period of the Korea-United
115 States Air Quality Study (KORUS-AQ) campaign (1 May – 12 June 2016) in South Korea.



116 In this study, the optimal interpolation (OI) method with the Kalman filter was
117 applied in order to develop an operational air quality prediction system, since this method is
118 still useful and viable in terms of computational cost and performance. The performance of
119 the method is almost comparable to that of the three-dimensional variational (3DVAR)
120 method, as shown in Tang et al. (2017). More complex and advanced DA techniques are
121 currently being and will continue to be applied to current air quality prediction systems.
122 These works are now in progress.

123 In addition, this manuscript also discusses several practical issues frequently
124 encountered in the operational air quality predictions such as: i) DA of NO₂ mixing ratios for
125 accurate ozone prediction with a careful consideration of measurement artifacts; ii) the issue
126 of the nocturnal mixing layer height (MLH) for nocturnal predictions; iii) predictions of dust
127 episodes; iv) the use of non-static free parameters; and v) the influences of multiple
128 implementations of the DA before the actual predictions.

129 The details of the datasets and methodology used in this study are described in Sect.
130 2. The results of the developed operational chemical weather prediction system are discussed
131 in Sect. 3, and then a summary and conclusions are given in Sect. 4.

132

133 **2. Methodology**

134 The operational air quality prediction system was developed using the CMAQ model
135 along with meteorological inputs provided by the Weather Research and Forecasting (WRF)
136 model (Skamarock et al., 2008). The ICs for the CMAQ model simulations were prepared via
137 the DA method using satellite-retrieved and ground-based observations. The performances of
138 the developed prediction system were evaluated using ground in-situ data. The models, data,
139 and DA technique are described in detail in the following sections.



140 **2.1 Meteorological and chemistry-transport modeling**

141 **2.1.1 WRF model simulations**

142 The WRF model has been developed for providing mesoscale numerical weather
143 prediction (NWP). It has also been used to provide meteorological input fields for CTM
144 simulations (Appel et al., 2010; Chemel et al., 2010; Foley et al., 2010; Lee et al., 2016; Park
145 et al., 2014). In this study, WRF v3.8.1 with the Advanced Research WRF (ARW) dynamic
146 core was applied to prepare the meteorological inputs for the CMAQ model simulations. The
147 National Centers for Environmental Prediction Final Analysis data (NCEP FNL) were chosen
148 for the ICs and boundary conditions (BCs) for the WRF simulations. In order to minimize
149 meteorological field error, the objective analysis (OBSGRID) nudging was conducted using
150 the NCEP Automated Data Processing (ADP) global upper-air/surface observational weather
151 data. The model domain for the WRF simulations covers Northeast Asia with a horizontal
152 resolution of $15 \times 15 \text{ km}^2$, having a total of 223 latitudinal and 292 longitudinal grid cells.
153 The size of the WRF domain is slightly larger than that of the CMAQ domain, as shown in
154 Fig. 1. The meteorological data also have 27 vertical layers from the surface (1000 hPa) to 50
155 hPa.

156

157 **2.1.2 CMAQ model simulations**

158 The CMAQ v5.1 model was used to estimate the concentrations of the atmospheric
159 chemical species over the domain, as shown in Fig. 1. The CMAQ domain has 204 latitudinal
160 and 273 longitudinal grid cells in total, and also has a $15 \times 15 \text{ km}^2$ horizontal resolution and
161 27 sigma vertical layers. For anthropogenic emissions, KORUS v1.0 emissions (Woo et al.,



162 2012) were used. The KORUS v1.0 emissions cover almost all of Asia, and are based on
163 three emission inventories: the Comprehensive Regional Emissions inventory for
164 Atmospheric Transport Experiment (CREATE) for East Asia excluding Japan; the Model
165 Inter-Comparison Study for Asia (MICS-Asia) for Japan; and the Studies of Emissions and
166 Atmospheric Composition, Clouds and Climate Coupling by Regional Surveys (SEAC4RS)
167 for South and Southeast Asia.

168 Biogenic emissions were prepared by running the Model of Emissions of Gases and
169 Aerosols from Nature (MEGAN v2.1; Guenther et al., 2006, 2012) with a grid size identical
170 to that of the CMAQ model simulations. For the MEGAN simulations, the MODIS land
171 cover data (Friedl et al., 2010) and improved leaf area index (LAI) based on MODIS datasets
172 (Yuan et al., 2011) were utilized. Pyrogenic emissions were obtained from the Fire Inventory
173 from NCAR (FINN; Wiedinmyer et al., 2006, 2011). The lateral BCs for the CMAQ model
174 simulations were prepared using the global model results of the Model for Ozone and Related
175 chemical Tracers version 4 (MOZART-4; Emmons et al., 2010) at every 6 hours. The
176 mapping and re-gridding of the MOZART-4 data were conducted by matching the CMAQ
177 grid information.

178

179 **2.2 Observation data**

180 **2.2.1. Satellite-based observations**

181 A Korean geostationary satellite of Communication, Ocean, and Meteorological
182 Satellite (COMS) was launched on 26 June in 2010 over the Korean Peninsula. The COMS is
183 a geostationary orbit satellite and it is stationed at an altitude of approximately 36,000 km at a
184 latitude of 36°N and a longitude of 128.2°E with a horizontal coverage of 2500 × 2500 km²
185 (refer to Fig. 1). Among the three payloads of the COMS, Geostationary Ocean Color Image



186 (GOCI) is the first multi-channel ocean color sensor with visible and near infrared channels.
187 The GOCI instrument provides hourly spectral images with a spatial resolution of 500×500
188 m^2 from 00:30 to 07:30 Coordinated Universal Time (UTC) for eight spectral (6 visible and 2
189 near-infrared) channels at 412, 443, 490, 555, 660, 680, 745, and 865 nm.

190 The Yonsei aerosol retrieval (YAER) algorithm for the GOCI sensor was initially
191 developed by Lee et al. (2010) to retrieve the aerosol optical properties (AOPs) over ocean
192 areas, and was then improved by expanding to consider non-spherical aerosol optical
193 properties (Lee et al., 2012). Choi et al. (2016) further extended the algorithm for application
194 to land surfaces, and the algorithm was referred to as the GOCI YAER version 1 algorithm.
195 With the GOCI YAER algorithm, hourly Aerosol Optical Depths (AODs) at 550 nm were
196 produced over East Asia. Choi et al. (2016) compared the retrieved GOCI AODs with other
197 satellite-retrieved and ground-based observations, and found several errors in the cloud
198 masking and surface reflectances. These errors were corrected in the recently updated second
199 version of the GOCI YAER algorithm (Choi et al., 2018), which used the updated cloud
200 masking and more accurate surface reflectances. In this study, the most recent GOCI AOD
201 products from the GOCI YAER version 2 algorithm were used.

202

203 **2.2.2. Ground-based observations**

204 In addition to the satellite data, ground-based observations in South Korea and China
205 were also collected for use in the operational air quality prediction system for PM and gas-
206 phase pollutants. The orange, red, and blue dots in Fig. 1 represent the ground-based
207 observation sites in China, Air Korea, and super-site stations in South Korea, respectively.
208 These observations provide real-time concentrations of criteria species such as PM_{10} , $\text{PM}_{2.5}$,



209 CO, O₃, SO₂, and NO₂.

210 Throughout the period of the KORUS-AQ campaign, ground-based observation data
211 were obtained from 1514 stations in China, 264 Air Korea stations, and seven super-site
212 stations in South Korea. In this study, 80 % of the ground-based observations in China and
213 Air Korea stations in South Korea were randomly selected for use in the prediction system.
214 The other 20 % of the data and super-site observations were used to evaluate the
215 performances of the developed air quality prediction system.

216 In addition, AERosol RObotic NETwork (AERONET) AODs were used to conduct an
217 independent evaluation of the air quality prediction system. AERONET is a federated global
218 ground-based sun photometer network (Holben et al., 1998). Cloud-screened and quality-
219 assured level 2.0 AODs for the AERONET were used in this study.

220

221 **2.3 Operational air quality prediction system**

222 In the present study, the operational air quality prediction system was developed by
223 adjusting the ICs for the CMAQ model simulations based on DA with satellite-retrieved and
224 ground-measured observations. Two parallel WRF-CMAQ model runs were conducted. The
225 first experiment that involved adjusting ICs via DA is referred to as DA RUN (see Fig. 2). In
226 order to evaluate the prediction system, a second experiment, in which the ICs were
227 originated from the previous CMAQ model simulations without assimilations, was also
228 conducted. This CMAQ run is referred to as BASE RUN.

229

230 **2.3.1. AOD calculations**

231 CMAQ AODs are calculated by integrating the aerosol extinction coefficient (σ_{ext})



232 using the following equation:

233

$$234 \quad \text{AOD}(\lambda) = \int_0^z \sigma_{\text{ext}}(\lambda) \, dz \quad (1)$$

235

236 where z represents the vertical height; σ_{ext} is defined as the sum of the absorption
237 coefficient (σ_{abs}) and the scattering coefficient (σ_{sca}); and σ_{abs} and σ_{sca} can be estimated
238 by Eqns (3) and (4), respectively, as shown below:

239

$$240 \quad \sigma_{\text{ext}}(\lambda) = \sigma_{\text{abs}}(\lambda) + \sigma_{\text{sca}}(\lambda) \quad (2)$$

$$241 \quad \sigma_{\text{abs}}(\lambda) [\text{Mm}^{-1}] = \sum_i^n \sum_j^m \{ (1 - \omega_{ij}(\lambda)) \cdot \beta_{ij}(\lambda) \cdot f_{ij}(\text{RH}) \cdot [C]_{ij} \} \quad (3)$$

$$242 \quad \sigma_{\text{sca}}(\lambda) [\text{Mm}^{-1}] = \sum_i^n \sum_j^m \{ \omega_{ij}(\lambda) \cdot \beta_{ij}(\lambda) \cdot f_{ij}(\text{RH}) \cdot [C]_{ij} \} \quad (4)$$

243

244 where i and j denote the particulate species and size bin (or particle mode), respectively;
245 $\omega_{ij}(\lambda)$ is the single scattering albedo; $\beta_{ij}(\lambda)$ is the mass extinction efficiency (MEE) of
246 particulate species i for the size bin or particle mode j ; $[C]_{ij}$ is the concentration of
247 particulate species including $(\text{NH}_4)_2\text{SO}_4$, NH_4NO_3 , black carbon, organic aerosols (OA),
248 mineral dust, and sea-salt aerosols; RH is the relative humidity; and $f_{ij}(\text{RH})$ is the
249 hygroscopic factor.

250 Here, the single scattering albedo (ω) refers to the fraction (portion) of the scattering
251 over total extinction. In this work, σ_{ext} was estimated using β and $f(\text{RH})$, as suggested by
252 Chin et al. (2012). Park et al. (2014) and Lee et al. (2016) found that the values reported by
253 Chin et al. (2012) produced the best results in estimating AODs at 550 nm over East Asia.
254 The calculated AODs were used in the air quality prediction system in order to prepare the



255 ICs for the PM predictions.

256

257 **2.3.2. Data assimilation (DA)**

258 The ground-based observations, together with GOCI-derived AODs, were used to
259 prepare the ICs for the operational air quality predictions with the CMAQ model simulations.
260 In order to achieve this, the following steps were taken: (i) the CMAQ-calculated
261 concentrations of CO, O₃, and SO₂ were combined with the concentrations of CO, O₃, and
262 SO₂ obtained from ground-based observations in South Korea (Air Korea) and China; (ii) the
263 CMAQ-calculated AODs were assimilated with the GOCI AODs; (iii) the assimilated AODs
264 were converted into PM₁₀; (iv) the converted PM₁₀ was again assimilated at the surface in
265 South Korea and China; and (v) after the DA at the surface, the ratios of the assimilated
266 species concentrations to the original CMAQ-simulated concentrations were applied so as to
267 the adjust vertical profiles of the chemical species above the surface. In the operational
268 prediction system, the DA cycle is 24 hours and the assimilation takes place every day at
269 00:00 UTC (refer to Fig. 3).

270 The optimal interpolation (OI) method with the Kalman filter was chosen in the
271 operational air quality prediction system. The OI method was originally used for
272 meteorological applications (Lorenc, 1986), and has also been used in the assimilations for
273 trace gases (Khattatov et al., 1999, 2000; Lamarque et al., 1999; Levelt et al., 1998). Recently,
274 the OI technique has also been applied to aerosol fields (Collins et al., 2001; Yu et al., 2003;
275 Generoso et al., 2007; Adhikary et al., 2008; Carmichael et al., 2009; Chung et al., 2010; Park
276 et al., 2011; Tang et al., 2015, 2017).

277 Aerosol assimilation using the OI method was first applied by Collins et al. (2001) as



278 follows:

279

$$280 \quad \tau'_m = \tau_m + \mathbf{K}(\tau_o - \mathbf{H}\tau_m) \quad (5)$$

$$281 \quad \mathbf{K} = \mathbf{B}\mathbf{H}^T(\mathbf{H}\mathbf{B}\mathbf{H}^T + \mathbf{O})^{-1} \quad (6)$$

$$282 \quad \mathbf{O} = [(f_o\tau_o)^2 + (\epsilon_o)^2]\mathbf{I} \quad (7)$$

$$283 \quad \mathbf{B}(d_x, d_z) = [(f_m\tau_m)^2 + (\epsilon_m)^2]\exp\left[-\frac{d_x^2}{2l_{mx}^2}\right]\exp\left[-\frac{d_z^2}{2l_{mz}^2}\right] \quad (8)$$

284

285 where τ'_m , τ_m , and τ_o represent the assimilated products by the OI method, the modeled
286 values, and the observed values, respectively; \mathbf{K} is the Kalman gain matrix; \mathbf{H} is the
287 observation operator (or forward operator), which is an interpolator from model to
288 observation space; \mathbf{B} and \mathbf{O} are the background and observation error covariance matrices,
289 respectively; $(\cdot)^T$ denotes the transpose of a matrix; f_o is the fractional error in the
290 observation-retrieved value; ϵ_o is the minimum root mean square error in the observation-
291 retrieved values; f_m is the fractional error in the model estimates; ϵ_m is the minimum root
292 mean square error in the model estimates; d_x is the horizontal distance between two model
293 grid points; l_{mx} is the horizontal correlation length scale for the errors in the model; d_z is
294 the vertical distance between two model grid points; and l_{mz} is the vertical correlation
295 length scale for the errors in the model. In this work, the OI technique was applied for the DA
296 of atmospheric gaseous species as well as particulate species.

297 Six free parameters (f_m , f_o , ϵ_m , ϵ_o , l_{mx} , and l_{mz}) were used to calculate the error
298 covariance matrices of the observations and model, the mathematical formalisms of which
299 are described in Eq. (7) and (8), respectively. Several previous studies have used fixed values
300 for free parameters (Collins et al., 2001; Yu et al., 2003; Adhikary et al., 2008; Chung et al.,



2010). These runs are called “static” runs. In contrast to those previous studies, “non-static” free parameters were applied in this study by minimizing the differences between the assimilated values and observations via an iterative process at each assimilation time step. This non-static free parameter scheme is possible due to the fact that the OI technique with the Kalman filter is much less costly in terms of computation time than other DA techniques, such as the 3-D or 4-D variational methods. This is another advantage of using the OI technique in this system. It typically takes less than 20 minutes with a workstation environment (dual Intel Xeon 2.40 GHz processor).

309

2.3.3. Allocation of the assimilated PM₁₀ & PM_{2.5} into particulate composition

In the procedure of operational DA, PM₁₀ was assimilated in this study, because the PM₁₀ data were more plentiful than PM_{2.5}. The assimilated PM₁₀ then needs to be allocated into the PM composition for the CMAQ-model prediction runs. In order to achieve this, the differences between the assimilated PM₁₀ and background PM₁₀ (ΔPM_{10}) were first calculated. Then, $\Delta PM_{2.5}$ was estimated using the ratios of PM_{2.5} to PM₁₀ from the background CMAQ model runs (i.e., $\Delta PM_{2.5} = \Delta PM_{10} \times PM_{2.5} / PM_{10}$). $\Delta PM_{2.5}$ was then allocated to the PM_{2.5} composition according to the comparison between two PM_{2.5} compositions observed at the seven super-sites and simulated from the CMAQ model runs over South Korea. Both of the compositions are shown in Fig. 4. In Fig. 4, “PM OTHERS” indicates the remaining particulate matter species after excluding sulfate, nitrate, ammonium, organic aerosol (OA), and elementary carbon (EC). The PM OTHERS occupies 25 % of the total PM_{2.5} observed at super-sites. The other fraction, $\Delta PM_{10} \times (1 - PM_{2.5} / PM_{10})$, was also distributed into the coarse-mode particles (PM_{2.5-10}) as crustal elements.



324 **3. Results and discussions**

325 The performances of the air quality prediction system were evaluated by comparing
326 them with ground-based observations from the Air Korea network and super-site stations in
327 South Korea. Several sensitivity analyses were also conducted in order to assess the
328 influences of the DA time-intervals on the accuracy of the air quality prediction.

329

330 **3.1. Evaluation of the air quality prediction system**

331 **3.1.1. Time-series analysis**

332 Figure 5 shows the time-series plots of PM₁₀, PM_{2.5}, CO, O₃, and SO₂ concentrations
333 from the BASE RUN and the DA RUN. Here, the observation data (OBS) obtained from the
334 Air Korea network were compared with the results of the two sets of the CMAQ model
335 simulations, i.e., (1) BASE RUN and (2) DA RUN. As mentioned previously, 20% of the Air
336 Korea observations used in the evaluation were randomly selected during the period of the
337 KORUS-AQ campaign. The other 80 % of the Air Korea data were used in the DA at 00:00
338 UTC. For the forecast hours from 01:00 to 23:00 UTC, all of the ground observations (254
339 Air Korea and seven super-site stations) were used to evaluate the performances of the
340 developed air quality prediction system. As shown in Fig. 5, we achieved some improvements
341 in the prediction performances by applying the ICs to the CMAQ model simulations. The
342 BASE RUN significantly under-predicted PM₁₀, PM_{2.5}, and CO while the DA RUN produced
343 concentrations that were more consistent with the observations than those of the BASE RUN.

344 In case of CO, the observed CO mixing ratios were about three times higher than
345 those from the BASE RUN. These large differences are well known, and have been attributed
346 to the underestimated emissions of CO (Heald et al., 2004). However, when the DA was



347 applied, the predictions of the CO mixing ratios improved. Similarly, the performances of the
348 PM₁₀ and PM_{2.5} predictions improved with the application of the DA. Unlike PM₁₀, PM_{2.5},
349 and CO, the O₃ mixing ratios and its diurnal trends from both the BASE RUN and DA RUN
350 tend to be well-matched with the observations. By contrast, the poorest performances of the
351 BASE RUN and the DA RUN were shown for SO₂.

352 In addition, a dust event took place between 6 May and 8 May. This event is captured
353 by the DA RUN (check red peaks in Fig. 5(a) and (b)), while the BASE RUN cannot capture
354 this dust event. This demonstrates the capability of the current system to possibly predict dust
355 events in South Korea. In the DA RUN, dust information is provided into the CMAQ model
356 runs through both/either GOCI AOD and/or ground PM observations measured along the dust
357 plume tracks.

358 The effectiveness of the DA with prediction time was also analyzed by calculating
359 the aggregated average concentrations of atmospheric species (see Figs. 6, 7, and 9). Fig. 6
360 depicts the CMAQ-calculated average concentrations of PM₁₀, PM_{2.5}, CO, and SO₂ against
361 the Air Korea observations. Our air quality prediction system re-generated relatively well-
362 matched concentrations for PM₁₀, PM_{2.5}, and CO from the DA RUN.

363 Figure 7 shows the case of ozone. The ozone mixing ratios from the DA RUN in Fig.
364 7(a) were reasonably consistent with the observations at 00:00 UTC, but disagreed with those
365 between 04:00 and 09:00 UTC (13:00 and 18:00 KST), when solar insolation is the most
366 intense. This may be attributed to the chemical imbalances between ozone production and
367 ozone destruction (or titration). However, if CMAQ NO₂ was assimilated with ground-based
368 observations in South Korea (Air Korea) and China, the predicted ozone mixing ratios
369 became substantially closer to the observations, as shown in Fig. 7(b). This is clearly due to



370 the fact that NO_x is an important precursor of ozone. In the prediction of the ozone mixing
371 ratios, both 1-hr peak ozone (around 15:00 KST) and 8-hr averaged ozone mixing ratios
372 (between 9:00 and 17:00 KST) are important. Fig. 7 clearly shows that the prediction
373 accuracies of both the ozone mixing ratios were improved after the DA of NO_2 mixing ratios.

374 Although the DA for NO_2 provided better ozone predictions, one should take caution
375 in using the NO_2 observations. The NO_2 mixing ratios measured at Air Korea sites are known
376 to be contaminated by other nitrogen gases such as nitric acid (HNO_3), peroxyacetyl nitrates
377 (PANs), and alkyl nitrates (ANs), since the Air Korea NO_2 mixing ratios are measured
378 through a chemiluminescent method with catalysts of gold or molybdenum oxide at high
379 temperatures. These are known to be “ NO_2 measurement artifacts” (Jung et al., 2017), which
380 is one of the reasons that the DA of NO_2 was not shown in Fig. 6. The NO_2 mixing ratios are
381 corrected from the Air Korea NO_2 data, and are then used to prepare the ICs via the DA for
382 more accurate ozone and NO_2 predictions. Currently, such corrections of the observed NO_2
383 mixing ratios are being standardized with more sophisticated year-long NO_2 measurements.
384 After the corrections of the NO_2 measurement artifacts, more evolved schemes of ozone and
385 NO_2 predictions will be possible in the future. As shown in Fig. 7, about a 20% reduction
386 (average fraction of non- NO_2 mixing ratios in the observed NO_2 mixing ratios) was made for
387 these demonstration runs (Jung et al., 2017).

388 Another practical issue is now discussed. Although the assimilation with the
389 observed NO_2 mixing ratios can enhance the accuracy of the predictions of the daytime ozone
390 mixing ratios, the nighttime ozone mixing ratios tend to be consistently over-predicted in the
391 aggregated plot of the ozone mixing ratios at the observation sites (see Fig. 7). This is
392 believed to be caused by underestimation of the mixing layer height (MLH). Figure 8 shows a



393 comparison between lidar-measured MLH (black dashed line) and WRF-calculated MLH
394 (with the option of the Yonsei University (YSU) planetary boundary layer scheme) (Hong et
395 al., 2006; see red line). As shown in Fig. 8, the nocturnal lidar-measured MLH is about two
396 times higher than the nocturnal WRF-calculated MLH as measured at a lidar site inside the
397 campus of Seoul National University (SNU) in Seoul. This is a common and well-defined
398 phenomenon in East Asia. Such underestimated MLH in the model tends to compress the
399 ozone molecules within the mixing layer during the nighttime, which leads to consistently
400 over-predicted nocturnal ozone mixing ratios.

401 Although the correct predictions of the daytime ozone mixing ratios are substantially
402 more important, it is also worth trying to achieve correct predictions of the nocturnal ozone
403 mixing ratios. Correct predictions of the nocturnal ozone mixing ratios strongly depend on
404 the correct estimation of the MLH. Currently, efforts are being made in two directions. First,
405 a modified MLH (or PBL) scheme in the meteorological model is currently being studied.
406 The other area of study is that the WRF-calculated MLH can be “bias-corrected” to match the
407 observed MLHs in the interface (MCIP) between a MET model (e.g., WRF) and a CTM
408 model (e.g., CMAQ). These efforts are now underway as well.

409 In this work, the aerosol composition (such as EC, OA, sulfate, nitrate, and
410 ammonium) was further compared with the composition observed at the super-sites shown in
411 Fig. 9. As shown in Fig. 9, agreement was observed between the DA RUN and observations
412 for all of the major PM constituents. Again, this is another strong capability of our system for
413 predicting not only particle mass, but also the “chemical composition” of particulate matters.

414

415 **3.1.2. Spatial distribution**



416 Figure 10 shows the spatial distributions of PM and chemical species throughout the
417 entire period of the KORUS-AQ campaign over the Seoul Metropolitan Area (SMA).
418 Noticeable improvements are observed to have been achieved in the spatial distributions by
419 applying the ICs into the CMAQ model simulations, particularly for PM₁₀ (Fig. 10a), PM_{2.5}
420 (Fig. 10b), and CO (Fig. 10c). As shown in Fig. 10, the under-predicted concentrations of
421 PM₁₀, PM_{2.5}, and CO were adjusted to concentrations closer to the observations. In case of
422 SO₂ (see Fig. 10d), the DA RUN produced better agreement with the observations than the
423 BASE RUN, but there were still under-predicted SO₂ concentrations over the northeastern
424 part of the SMA.

425 By contrast, relatively lower ozone mixing ratios from the DA RUN against the
426 BASE RUN were found in the southwestern part of the SMA (see Fig. 10e). Due to the
427 nonlinear relationship between NO_x and O₃, high mixing ratios (or emissions) of NO_x in the
428 SMA can lead to depletion of ozone. In these runs, the precursors of ozone such as NO_x and
429 VOCs were excluded in the preparation of the ICs for CMAQ model simulations. Again, this
430 is because the Air Korea NO₂ mixing ratios are contaminated by several reactive nitrogen
431 species, so the data cannot be directly used in the assimilation procedures. In case of VOCs, a
432 limited number of datasets is available in South Korea for the DA. Improvements in the
433 prediction of ozone mixing ratios can be achieved when the NO₂ mixing ratios are corrected
434 and a sufficient number of VOCs data (possibly from satellite data in the future) is available.

435

436 3.1.3. Statistical analysis

437 In order to achieve better understanding of the performances of the DA RUN,
438 analyses of statistical variables such as index of agreement (IOA), Pearson's correlation



439 coefficient (R), root mean square error (RMSE), and mean bias (MB) were conducted using
440 observations from the Air Korea stations for PM₁₀, PM_{2.5}, CO, SO₂, and O₃ (see Fig. 11).
441 Definitions of the statistical variables are given in Appendix A.

442 After the applications of the ICs, both RMSE and MB became lower, while the
443 correlation coefficient became higher for the entire predictions. In addition, it was found that
444 the differences between the BASE RUN and the DA RUN tended to diminish as the
445 prediction time progressed. The results of the statistical analysis are listed in Table 1. The
446 results of the DA RUN were reasonably consistent with the observations for PM₁₀ (IOA =
447 0.60; R= 0.40; RMSE = 34.87; MB = -13.54) and PM_{2.5} (IOA = 0.71; R= 0.53; RMSE = 17.
448 83; MB = -2.43), as compared to the BASE RUN for PM₁₀ (IOA = 0.51; R= 0.34; RMSE =
449 40.84; MB = -27.18) and PM_{2.5} (IOA = 0.67; R= 0.51; RMSE = 19.24; MB = -9.9). In terms
450 of bias, an improvement was found for CO: MB = -0.036 for the DA RUN and MB = -0.27
451 for the BASE RUN. Regarding O₃ and SO₂, the DA RUN showed slightly better
452 performances than the BASE RUN.

453 Table 2 presents the results of the statistical analysis at 00:00 UTC when the DA was
454 conducted, with the results clearly showing how much closer the DA makes the CMAQ-
455 calculated chemical concentrations to the observed concentrations. Collectively, the DA
456 improved model accuracy by a large degree in terms of R, particularly for PM₁₀ (R:
457 0.3→0.75; slope: 0.17→0.66) and O₃ (R: 0.09→0.61; slope: 0.07→0.42). In addition, for all
458 species, MB and RMSE decreased significantly with the DA RUN as compared with the
459 BASE RUN.

460

461 **3.2. Sensitivity test of DA time-interval**



462 **3.2.1. AOD**

463 In this section, a sensitivity analysis was conducted with different implementation
464 time-intervals of the DA (i.e., 24, 6, and 3 hours) for AOD (refer to Fig. 12). As shown in Fig.
465 12, more frequent implementation of the DA is expected to make the predicted results closer
466 to the observations. Although the DA RUN with a shorter assimilation time-interval tends to
467 produce a better prediction, it is not always the most appropriate choice, since the shorter
468 assimilation time-interval results in increased computational cost. Therefore, an optimized
469 assimilation time-interval should be found to achieve the best performances from the given
470 DA system with the consideration of its own computational ability.

471

472 **3.2.2. PM and gases**

473 In addition, sensitivity analyses of the developed air quality prediction system to
474 multiple implementations of the DA with different time-intervals were also investigated for (a)
475 PM₁₀, (b) PM_{2.5}, (c) CO, (d) SO₂, and (e) O₃, shown in Fig. 13. Fig. 13 shows a soccer plot
476 analysis for BASE RUN (blue crosses) and DA RUNs with different DA time-intervals of 24
477 hours (OI; red circles), two hours (2-hr OI; black diamonds), and one hour (1-hr OI; dark-
478 green triangles). This set of testing was designed based on the fact that the performances are
479 expected to improve if the DAs are implemented multiple times prior to the actual predictions
480 at 00:00 UTC. Here, for the 2-hr OI run, the DA was implemented three times a day at 20:00,
481 22:00, and 00:00 UTC, while for the 1-hr OI run, the DA was implemented at 22:00, 23:00,
482 and 00:00 UTC. The performances of all of the chemical species excluding ozone improved,
483 as expected, with DA RUNs with more frequent and longer DA time-intervals (i.e., three-
484 times implementation with a 2-hr time-interval in our cases). In case of ozone, the best



485 performance was found for the air quality prediction system with the DA time-interval of 24-
486 hr.

487 Unsurprisingly, more frequent DAs prior to the actual prediction mode (i.e., before
488 00:00 UTC in our system) with a longer time-interval (such as 2-hr) will be computationally
489 costly. There will certainly be a “trade-off” between the precision of air quality prediction and
490 the computational cost. The system should be designed under the consideration of these two
491 factors.

492

493 **4. Summary and conclusions**

494 In this study, an operational air quality prediction system was developed by preparing
495 the ICs for CMAQ model simulations using GOCI AODs and ground-based observations of
496 PM₁₀, CO, ozone, and SO₂ during the period of the KORUS-AQ campaign (1 May – 12 June
497 2016) in South Korea. The major advantages of the developed air quality prediction system
498 are its comprehensiveness in predicting the ambient concentrations of both gaseous and
499 particulate species (including PM composition) as well as its powerfulness in terms of
500 computational cost.

501 The performances of the developed prediction system were evaluated using ground
502 in-situ observation data. The CMAQ model runs with the ICs (DA RUN) showed higher
503 consistency with the observations of almost all of the chemical species, including PM
504 composition (sulfate, nitrate, ammonium, OA, and EC) and atmospheric gases (CO, ozone,
505 and SO₂), than the CMAQ model runs without the ICs (BASE RUN). Particularly for CO, the
506 DA was able to remarkably improve the model performances, while the BASE RUN
507 significantly under-predicted the CO concentrations (predicting about one-third of the



508 observed values). In case of ozone, both the BASE RUN and DA RUN were in close
509 agreement with observations. More reliable predictions of ozone mixing ratios will be
510 achieved via the DA of the observed NO₂ mixing ratios and the corrections of model-
511 simulated mixing layer height (MLH). For SO₂, the performances of both the BASE RUN
512 and the DA RUN were somewhat poor. Regarding this issue, more accurate SO₂ emissions
513 are required to achieve better SO₂ predictions, and these can be estimated through inverse
514 modeling using satellite data (e.g., Lee et al., 2011). The adjustments of both ICs and
515 emissions may be able to improve the performances of the air quality prediction system, and
516 this will be examined in future studies.

517 Moreover, the developed air quality prediction system will be upgraded by using the
518 new observation data that will be retrieved after 2020 from the Geostationary Environment
519 Monitoring Spectrometer (GEMS) with a high spatial resolution of $7 \times 8 \text{ km}^2$ as well as a
520 high temporal resolution of 1-hour over a large part of Asia. In addition, the current DA
521 technique of the OI with the Kalman filter can also be upgraded with the use of more
522 advanced DA methods such as variational techniques of 3DVAR and 4DVAR methods, as
523 well as with the ensemble Kalman filter (EnK) method. These research endeavors are
524 currently underway.

525 In conjunction with improving the air quality modeling system, artificial intelligence
526 (AI)-based air quality prediction systems are also currently being developed in several ways
527 (e.g., H. S. Kim et al., 2019). Both the CTM-based and AI-based air quality prediction
528 systems will be combined so as to ultimately enable more accurate air quality forecasts over
529 South Korea for Korean citizens. This is the ultimate goal of our research.



530 **Code and data availability.** WRF v3.8.1 (doi:10.5065/D6MK6B4K) and CMAQ v5.1
531 (doi:10.5281/zenodo.1079909) models are both open-source and publicly available. Source
532 codes for WRF and CMAQ can be downloaded at [http://www2.mmm.ucar.edu/wrf/users/
533 downloads.html](http://www2.mmm.ucar.edu/wrf/users/downloads.html) and <https://github.com/USEPA/CMAQ>, respectively. Data from the KORUS-
534 AQ field campaign can be downloaded from the KORUS-AQ data archive ([http://www-
535 air.larc.nasa.gov/missions/korus-aq](http://www-air.larc.nasa.gov/missions/korus-aq)). Other data were acquired as follows. Ground-based
536 observation data were downloaded from the Air Korea website (<http://www.airkorea.or.kr>) for
537 South Korea and <https://pm25.in> for China. AERONET data were downloaded from
538 <https://aeronet.gsfc.nasa.gov>. All codes related with the air quality prediction system can be
539 obtained by contacting K. Lee (lkh1515@gmail.com).

540

541 **Author contributions.** KL developed the model code, performed the simulations, and
542 analyzed the results. CHS directed the experiments. JY contributed to shape the research and
543 analysis. SL, MP, HH, and SYP helped analyze the results. MC, JK, YK, JHW, and SWK
544 provided and analyzed data applied in the experiments. KL prepared the manuscript with
545 contributions from all co-authors.

546

547 **Acknowledgments**

548 This research was supported by the National Strategic Project-Fine particle of the National
549 Research Foundation of Korea (NRF) of the Ministry of Science and ICT (MSIT), the
550 Ministry of Environment (MOE), and the Ministry of Health and Welfare (MOHW) (NRF-
551 2017M3D8A1092022). This work was also funded by the MOE as "Public Technology



552 Program based on Environmental Policy (2017000160001)” and was supported by a grant
553 from the National Institute of Environment Research (NIER), funded by the MOE of the
554 Republic of Korea (NIER-2019-01-01-028). Specially thanks to the entire KORUS-AQ
555 science team for their considerable efforts in conducting the campaign.



556 **APPENDIX A: FORMULAS FOR STATISTICAL EVALUATION INDICES**

557 The formulas used to evaluate the performances of the operational air quality prediction
558 system are defined as follows.

559

560 Index Of Agreement (IOA) = $1 - \frac{\sum_1^n (M - O)^2}{\sum_1^n (|M - \bar{O}| + |O - \bar{O}|)^2}$ (A1)

561

562 Correlation Coefficient (R) = $\frac{1}{(n-1)} \sum_1^n \left(\left(\frac{O - \bar{O}}{\sigma_o} \right) \left(\frac{M - \bar{M}}{\sigma_m} \right) \right)$ (A2)

563

564 Root Mean Square Error (RMSE) = $\sqrt{\frac{\sum_1^n (M - O)^2}{n}}$ (A3)

565

566 Mean Bias (MB) = $\frac{1}{n} \sum_1^n (M - O)$ (A4)

567

568 Mean Normalized Bias (MNB) = $\frac{1}{n} \sum_1^n \left(\frac{M - O}{O} \right) \times 100\%$ (A5)

569

570 Mean Normalized Error (MNE) = $\frac{1}{n} \sum_1^n \left(\frac{|M - O|}{O} \right) \times 100\%$ (A6)

571

572 Mean Fractional Bias (MFB) = $\frac{1}{n} \sum_1^n \left(\frac{M - O}{\frac{M + O}{2}} \right) \times 100\%$ (A7)

573



574

$$\text{Mean Fractional Error (MFE)} = \frac{1}{n} \sum_1^n \frac{|M - O|}{\left(\frac{M + O}{2}\right)} \times 100 \% \quad (\text{B8})$$

575

576 In Eqns. (A1) - (A8), M and O represent the model and observation data, respectively. N is
577 the number of data points and σ means the standard deviation. The overbars in the equations
578 indicate the arithmetic mean of the data. The units of RMSE and MB are the same as the unit
579 of data, while IOA and R are dimensionless statistical parameters.



580 **References**

- 581 Adhikary, B., Kulkarni, S., Dallura, A., Tang, Y., Chai, T., Leung, L. R., Qian, Y., Chung, C.
582 E., Ramanathan, V. and Carmichael, G. R.: A regional scale chemical transport modeling
583 of Asian aerosols with data assimilation of AOD observations using optimal interpolation
584 technique, *Atmospheric Environment*, 42(37), 8600–8615,
585 doi:10.1016/j.atmosenv.2008.08.031, 2008.
- 586 Appel, K. W., Roselle, S. J., Gilliam, R. C. and Pleim, J. E.: Sensitivity of the Community
587 Multiscale Air Quality (CMAQ) model v4.7 results for the eastern United States to
588 MM5 and WRF meteorological drivers, *Geoscientific Model Development*, 3, 169–188,
589 2010.
- 590 Bellouin, N., Boucher, O., Haywood, J. and Reddy, M. S.: Global estimate of aerosol direct
591 radiative forcing from satellite measurements, *Nature*, 438(7071), 1138–1141,
592 doi:10.1038/nature04348, 2005.
- 593 Bréon, F.-M., Tanré, D. and Generoso, S.: Aerosol Effect on Cloud Droplet Size Monitored
594 from Satellite, *Science*, 295(5556), 834–838, doi:10.1126/science.1066434, 2002.
- 595 Byun, D. and Schere, K. L.: Review of the Governing Equations, Computational Algorithms,
596 and Other Components of the Models-3 Community Multiscale Air Quality (CMAQ)
597 Modeling System, *Appl. Mech. Rev.*, 59(2), 51–77, doi:10.1115/1.2128636, 2006.
- 598 Byun, D. W. and Ching, J. K. S.: Science algorithms of the EPA models-3 community
599 multiscale air quality (CMAQ) modeling system, U.S. Environmental Protection Agency,
600 EPA/600/R-99/030 (NTIS PB2000-100561), 1999.
- 601 Carmichael, G. R., Sakurai, T., Streets, D., Hozumi, Y., Ueda, H., Park, S. U., Fung, C., Han,
602 Z., Kajino, M., Engardt, M., Bennet, C., Hayami, H., Sartelet, K., Holloway, T., Wang,
603 Z., Kannari, A., Fu, J., Matsuda, K., Thongboonchoo, N. and Amann, M.: MICS-Asia II:
604 The model intercomparison study for Asia Phase II methodology and overview of
605 findings, *Atmospheric Environment*, 42(15), 3468–3490,
606 doi:10.1016/j.atmosenv.2007.04.007, 2008.
- 607 Carmichael, G. R., Adhikary, B., Kulkarni, S., D’Allura, A., Tang, Y., Streets, D., Zhang, Q.,
608 Bond, T. C., Ramanathan, V., Jamroensan, A. and Marrapu, P.: Asian Aerosols: Current
609 and Year 2030 Distributions and Implications to Human Health and Regional Climate
610 Change, *Environ. Sci. Technol.*, 43(15), 5811–5817, doi:10.1021/es8036803, 2009.
- 611 Chemel, C., Sokhi, R. S., Yu, Y., Hayman, G. D., Vincent, K. J., Dore, A. J., Tang, Y. S., Prain,
612 H. D. and Fisher, B. E. A.: Evaluation of a CMAQ simulation at high resolution over the
613 UK for the calendar year 2003, *Atmospheric Environment*, 44(24), 2927–2939,
614 doi:10.1016/j.atmosenv.2010.03.029, 2010.
- 615 Choi, M., Kim, J., Lee, J., Kim, M., Park, Y.-J., Jeong, U., Kim, W., Hong, H., Holben, B.,
616 Eck, T. F., Song, C. H., Lim, J.-H. and Song, C.-K.: GOCI Yonsei Aerosol Retrieval
617 (YAER) algorithm and validation during the DRAGON-NE Asia 2012 campaign, *Atmos.*



- 618 Meas. Tech., 9(3), 1377–1398, doi:10.5194/amt-9-1377-2016, 2016.
- 619 Choi, M., Kim, J., Lee, J., Kim, M., Park, Y.-J., Holben, B., Eck, T. F., Li, Z. and Song, C. H.:
620 GOCI Yonsei aerosol retrieval version 2 products: an improved algorithm and error
621 analysis with uncertainty estimation from 5-year validation over East Asia, *Atmos. Meas.*
622 *Tech.*, 11(1), 385–408, doi:10.5194/amt-11-385-2018, 2018.
- 623 Chung, C. E., Ramanathan, V., Carmichael, G., Kulkarni, S., Tang, Y., Adhikary, B., Leung, L.
624 R. and Qian, Y.: Anthropogenic aerosol radiative forcing in Asia derived from regional
625 models with atmospheric and aerosol data assimilation, *Atmos. Chem. Phys.*, 10(13),
626 6007–6024, doi:10.5194/acp-10-6007-2010, 2010.
- 627 Collins, W. D., Rasch, P. J., Eaton, B. E., Khattatov, B. V., Lamarque, J.-F. and Zender, C. S.:
628 Simulating aerosols using a chemical transport model with assimilation of satellite
629 aerosol retrievals: Methodology for INDOEX, *J. Geophys. Res.*, 106(D7), 7313–7336,
630 doi:10.1029/2000JD900507, 2001.
- 631 Dehghani, M., Keshtgar, L., Javaheri, M. R., Derakhshan, Z., Conti, O., Gea, Zuccarello, P.
632 and Ferrante, M.: The effects of air pollutants on the mortality rate of lung cancer and
633 leukemia, *Molecular Medicine Reports*, 15(5), 3390–3397, 2017.
- 634 Emmons, L. K., Walters, S., Hess, P. G., Lamarque, J.-F., Pfister, G. G., Fillmore, D., Granier,
635 C., Guenther, A., Kinnison, D., Laepple, T., Orlando, J., Tie, X., Tyndall, G.,
636 Wiedinmyer, C., Baughcum, S. L. and Kloster, S.: Description and evaluation of the
637 Model for Ozone and Related chemical Tracers, version 4 (MOZART-4), *Geosci. Model*
638 *Dev.*, 3(1), 43–67, doi:10.5194/gmd-3-43-2010, 2010.
- 639 Foley, K. M., Roselle, S. J., Appel, K. W., Bhave, P. V., Pleim, J. E., Otte, T. L., Mathur, R.,
640 Sarwar, G., Young, J. O., Gilliam, R. C., Nolte, C. G., Kelly, J. T., Gilliland, A. B. and
641 Bash, J. O.: Incremental testing of the Community Multiscale Air Quality (CMAQ)
642 modeling system version 4.7, *Geosci. Model Dev.*, 3(1), 205–226, doi:10.5194/gmd-3-
643 205-2010, 2010.
- 644 Friedl, M. A., Sulla-Menashe, D., Tan, B., Schneider, A., Ramankutty, N., Sibley, A. and
645 Huang, X.: MODIS Collection 5 global land cover: Algorithm refinements and
646 characterization of new datasets, *Remote Sensing of Environment*, 114(1), 168–182,
647 doi:10.1016/j.rse.2009.08.016, 2010.
- 648 Generoso, S., Bréon, F.-M., Chevallier, F., Balkanski, Y., Schulz, M. and Bey, I.: Assimilation
649 of POLDER aerosol optical thickness into the LMDz-INCA model: Implications for the
650 Arctic aerosol burden, *J. Geophys. Res.*, 112(D2), D02311, doi:10.1029/2005JD006954,
651 2007.
- 652 Guenther, A., Karl, T., Harley, P., Wiedinmyer, C., Palmer, P. I. and Geron, C.: Estimates of
653 global terrestrial isoprene emissions using MEGAN (Model of Emissions of Gases and
654 Aerosols from Nature), *Atmospheric Chemistry and Physics*, 6(11), 3181–3210, 2006.



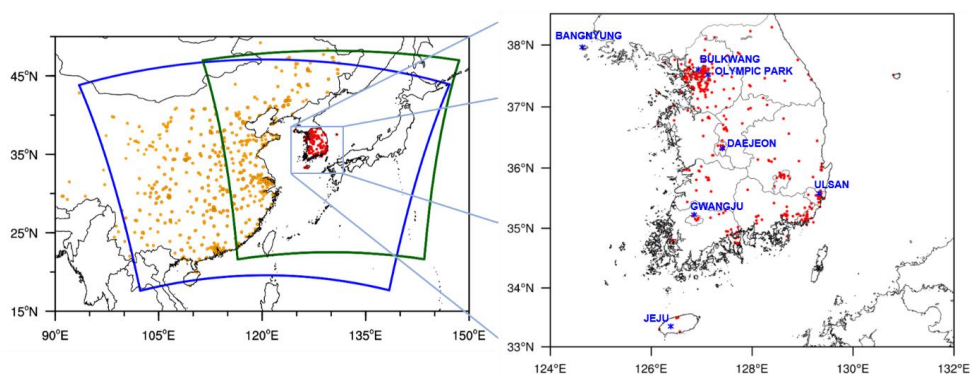
- 655 Guenther, A. B., Jiang, X., Heald, C. L., Sakulyanontvittaya, T., Duhl, T., Emmons, L. K. and
656 Wang, X.: The Model of Emissions of Gases and Aerosols from Nature version 2.1
657 (MEGAN2.1): an extended and updated framework for modeling biogenic emissions,
658 *Geosci. Model Dev.*, 5(6), 1471–1492, doi:10.5194/gmd-5-1471-2012, 2012.
- 659 Heald, C. L., Jacob, D. J., Jones, D. B. A., Palmer, P. I., Logan, J. A., Streets, D. G., Sachse,
660 G. W., Gille, J. C., Hoffman, R. N. and Nehrkorn, T.: Comparative inverse analysis of
661 satellite (MOPITT) and aircraft (TRACE-P) observations to estimate Asian sources of
662 carbon monoxide: COMPARATIVE INVERSE ANALYSIS, *Journal of Geophysical*
663 *Research: Atmospheres*, 109(D23), doi:10.1029/2004JD005185, 2004.
- 664 Holben, B. N., Eck, T. F., Slutsker, I., Tanré, D., Buis, J. P., Setzer, A., Vermote, E., Reagan, J.
665 A., Kaufman, Y. J., Nakajima, T., Lavenu, F., Jankowiak, I. and Smirnov, A.:
666 AERONET—A Federated Instrument Network and Data Archive for Aerosol
667 Characterization, *Remote Sensing of Environment*, 66(1), 1–16, doi:10.1016/S0034-
668 4257(98)00031-5, 1998.
- 669 Hong, S.-Y., Noh, Y. and Dudhia, J.: A New Vertical Diffusion Package with an Explicit
670 Treatment of Entrainment Processes, *Mon. Wea. Rev.*, 134(9), 2318–2341,
671 doi:10.1175/MWR3199.1, 2006.
- 672 IPCC: Climate Change 2013: The Physical Science Basis. The Fifth Assessment Report of
673 the Intergovernmental Panel on Climate Change, , Cambridge University Press,
674 Cambridge, United Kingdom and New York, NY, USA, 2013.
- 675 Jung, J., Lee, J., Kim, B. and Oh, S.: Seasonal variations in the NO₂ artifact from
676 chemiluminescence measurements with a molybdenum converter at a suburban site in
677 Korea (downwind of the Asian continental outflow) during 2015–2016, *Atmospheric*
678 *Environment*, 165, 290–300, doi:10.1016/j.atmosenv.2017.07.010, 2017.
- 679 Khaniabadi, Y. O., Goudarzi, G., Daryanoosh, S. M., Borgini, A., Tittarelli, A. and De Marco,
680 A.: Exposure to PM₁₀, NO₂, and O₃ and impacts on human health, *Environmental*
681 *Science and Pollution Research*, 24(3), 2781–2789, doi:10.1007/s11356-016-8038-6,
682 2017.
- 683 Khattatov, B. V., Gille, J. C., Lyjak, L. V., Brasseur, G. P., Dvortsov, V. L., Roche, A. E. and
684 Waters, J. W.: Assimilation of photochemically active species and a case analysis of
685 UARS data, *J. Geophys. Res.*, 104(D15), 18715–18737, doi:10.1029/1999JD900225,
686 1999.
- 687 Khattatov, B. V., Lamarque, J.-F., Lyjak, L. V., Menard, R., Levelt, P., Tie, X., Brasseur, G. P.
688 and Gille, J. C.: Assimilation of satellite observations of long-lived chemical species in
689 global chemistry transport models, *J. Geophys. Res.*, 105(D23), 29135–29144,
690 doi:10.1029/2000JD900466, 2000.
- 691 Lamarque, J.-F., Khattatov, B. V., Gille, J. C. and Brasseur, G. P.: Assimilation of
692 Measurement of Air Pollution from Space (MAPS) CO in a global three-dimensional



- 693 model, *J. Geophys. Res.*, 104(D21), 26209–26218, doi:10.1029/1999JD900807, 1999.
- 694 Lee, C., Martin, R. V., Donkelaar, A. van, Lee, H., Dickerson, R. R., Hains, J. C., Krotkov, N.,
695 Richter, A., Vinnikov, K. and Schwab, J. J.: SO₂ emissions and lifetimes: Estimates
696 from inverse modeling using in situ and global, space-based (SCIAMACHY and OMI)
697 observations, *Journal of Geophysical Research: Atmospheres*, 116(D6),
698 doi:10.1029/2010JD014758, 2011.
- 699 Lee, J., Kim, J., Song, C. H., Ryu, J.-H., Ahn, Y.-H. and Song, C. K.: Algorithm for retrieval
700 of aerosol optical properties over the ocean from the Geostationary Ocean Color Imager,
701 *Remote Sensing of Environment*, 114(5), 1077–1088, doi:10.1016/j.rse.2009.12.021,
702 2010.
- 703 Lee, J., Kim, J., Yang, P. and Hsu, N. C.: Improvement of aerosol optical depth retrieval from
704 MODIS spectral reflectance over the global ocean using new aerosol models archived
705 from AERONET inversion data and tri-axial ellipsoidal dust database, *Atmos. Chem.*
706 *Phys.*, 12(15), 7087–7102, doi:10.5194/acp-12-7087-2012, 2012.
- 707 Lee, S., Song, C. H., Park, R. S., Park, M. E., Han, K. M., Kim, J., Choi, M., Ghim, Y. S. and
708 Woo, J.-H.: GIST-PM-Asia v1: development of a numerical system to improve
709 particulate matter forecasts in South Korea using geostationary satellite-retrieved aerosol
710 optical data over Northeast Asia, *Geosci. Model Dev.*, 9(1), 17–39, doi:10.5194/gmd-9-
711 17-2016, 2016.
- 712 Levelt, P. F., Khattatov, B. V., Gille, J. C., Brasseur, G. P., Tie, X. X. and Waters, J. W.:
713 Assimilation of MLS ozone measurements in the global three-dimensional chemistry
714 transport model ROSE, *Geophys. Res. Lett.*, 25(24), 4493–4496,
715 doi:10.1029/1998GL900152, 1998.
- 716 Lorenc, A. C.: Analysis methods for numerical weather prediction, *Q.J.R. Meteorol. Soc.*,
717 112(474), 1177–1194, doi:10.1002/qj.49711247414, 1986.
- 718 Park, M. E., Song, C. H., Park, R. S., Lee, J., Kim, J., Lee, S., Woo, J.-H., Carmichael, G. R.,
719 Eck, T. F., Holben, B. N., Lee, S.-S., Song, C. K. and Hong, Y. D.: New approach to
720 monitor transboundary particulate pollution over Northeast Asia, *Atmos. Chem. Phys.*,
721 14(2), 659–674, doi:10.5194/acp-14-659-2014, 2014.
- 722 Park, R. S., Song, C. H., Han, K. M., Park, M. E., Lee, S.-S., Kim, S.-B. and Shimizu, A.: A
723 study on the aerosol optical properties over East Asia using a combination of CMAQ-
724 simulated aerosol optical properties and remote-sensing data via a data assimilation
725 technique, *Atmos. Chem. Phys.*, 11(23), 12275–12296, doi:10.5194/acp-11-12275-2011,
726 2011.
- 727 Penner, J. E., Dong, X. and Chen, Y.: Observational evidence of a change in radiative forcing
728 due to the indirect aerosol effect, *Nature*, 427(6971), 231–234, doi:10.1038/nature02234,
729 2004.



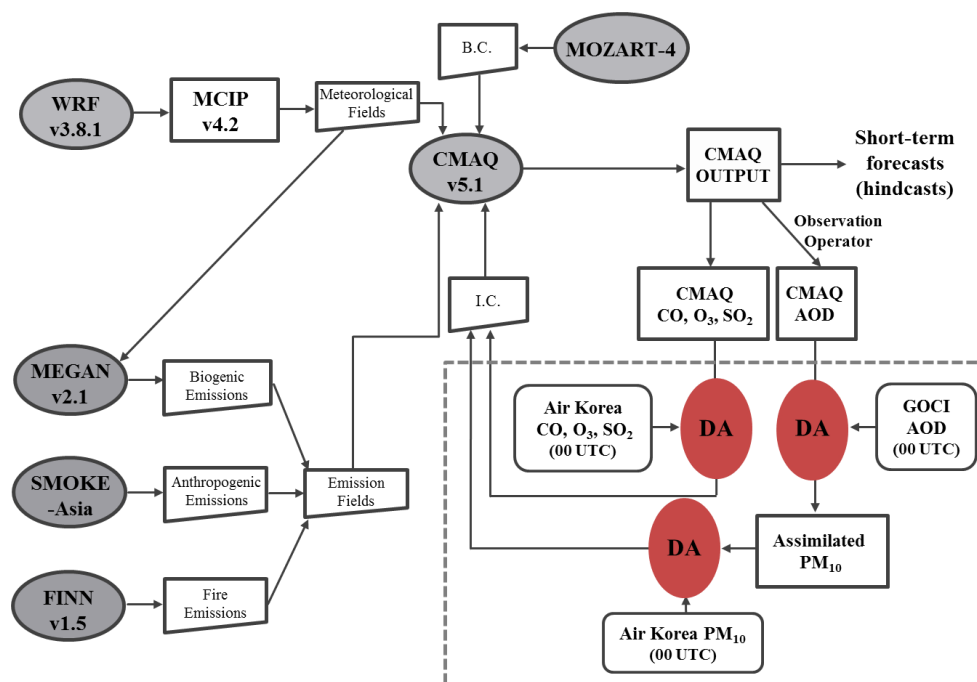
- 730 Scott, C. E., Rap, A., Spracklen, D. V., Forster, P. M., Carslaw, K. S., Mann, G. W., Pringle, K.
731 J., Kivekäs, N., Kulmala, M., Lihavainen, H. and Tunved, P.: The direct and indirect
732 radiative effects of biogenic secondary organic aerosol, *Atmos. Chem. Phys.*, 14(1),
733 447–470, doi:10.5194/acp-14-447-2014, 2014.
- 734 Skamarock, C., Klemp, B., Dudhia, J., Gill, O., Barker, D., Duda, G., Huang, X., Wang, W.
735 and Powers, G.: A Description of the Advanced Research WRF Version 3, ,
736 doi:10.5065/D68S4MVH, 2008.
- 737 Tang, Y., Chai, T., Pan, L., Lee, P., Tong, D., Kim, H.-C. and Chen, W.: Using optimal
738 interpolation to assimilate surface measurements and satellite AOD for ozone and PM2.5:
739 A case study for July 2011, *Journal of the Air & Waste Management Association*, 65(10),
740 1206–1216, doi:10.1080/10962247.2015.1062439, 2015.
- 741 Wiedinmyer, C., Quayle, B., Geron, C., Belote, A., McKenzie, D., Zhang, X., O’Neill, S. and
742 Wynne, K. K.: Estimating emissions from fires in North America for air quality
743 modeling, *Atmospheric Environment*, 40(19), 3419–3432,
744 doi:10.1016/j.atmosenv.2006.02.010, 2006.
- 745 Wiedinmyer, C., Akagi, S., Yokelson, R., Emmons, L., Al-Saadi, J., Orlando, J. and Soja, A.:
746 The Fire INventory from NCAR (FINN): A High Resolution Global Model to Estimate
747 the Emissions from Open Burning, *Geoscientific Model Development*, 625–641, 2011.
- 748 Yu, H., Dickinson, R. E., Chin, M., Kaufman, Y. J., Holben, B. N., Geogdzhayev, I. V. and
749 Mishchenko, M. I.: Annual cycle of global distributions of aerosol optical depth from
750 integration of MODIS retrievals and GOCART model simulations, *J. Geophys. Res.*,
751 108(D3), 4128, doi:10.1029/2002JD002717, 2003.
- 752 Yuan, H., Dai, Y., Xiao, Z., Ji, D. and Shangguan, W.: Reprocessing the MODIS Leaf Area
753 Index products for land surface and climate modelling, *Remote Sensing of Environment*,
754 115(5), 1171–1187, doi:10.1016/j.rse.2011.01.001, 2011.



755

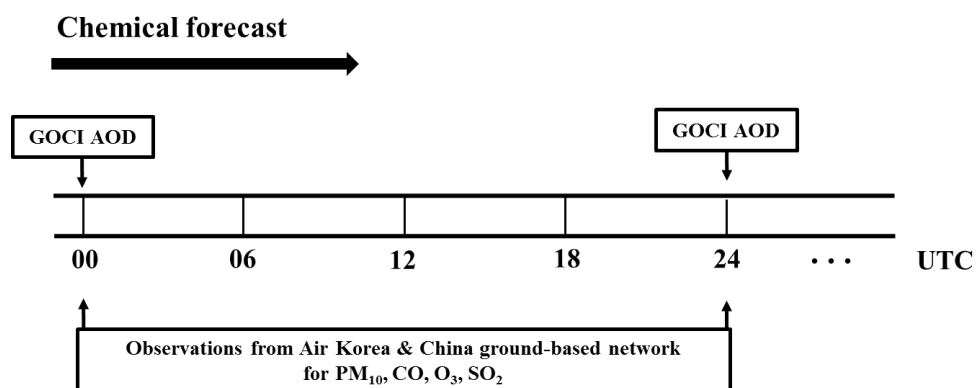
756 **Figure 1.** Domains of GOCI sensor (dark green line) and CMAQ model simulations (blue
757 line). Red-colored dots denote the locations of Air Korea sites in South Korea. Orange-
758 colored dots represent the locations of ground-based observation stations in China. Blue
759 stars show the locations of seven super-sites in South Korea. During the KORUS-AQ campaign,
760 observation data were obtained from 1514 stations in China as well as 264 Air Korea and
761 seven super-site stations in South Korea.

762



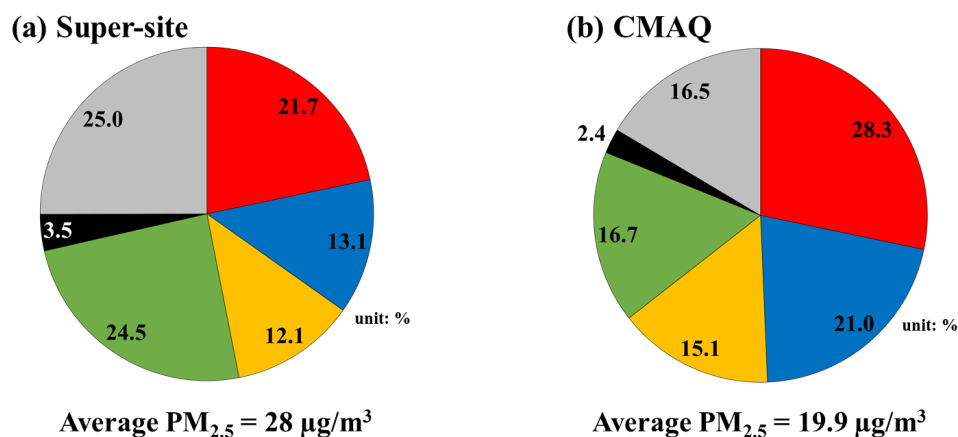
763

764 **Figure 2.** Schematic diagram of the Korean air quality prediction system developed in this
765 study. The initial conditions (ICs) of the CMAQ model simulations are prepared by
766 assimilating CMAQ outputs with satellite-retrieved and ground-measured observations. The
767 data process for preparing the ICs is shown in the box with gray-dashed lines.



768

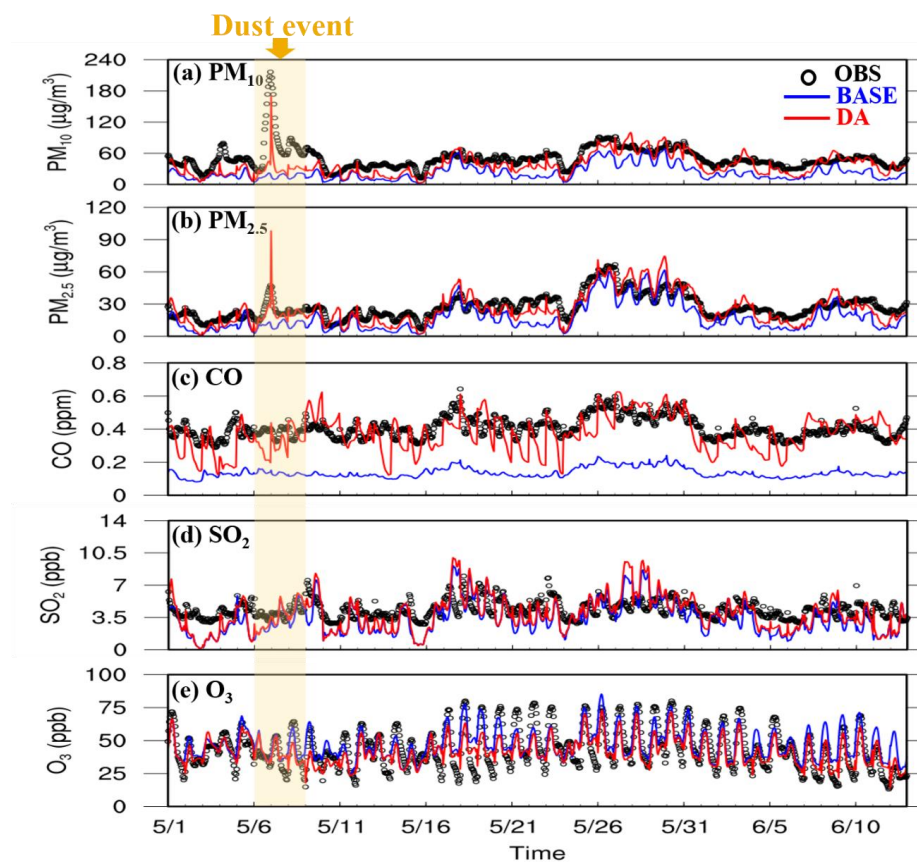
769 **Figure 3.** Schematic diagram of the Korean air quality prediction system for particulate
770 matter (PM) and gas-phase pollutants. The data assimilation (DA) cycle is 24 hours for both
771 PM and gas-phase pollutants such as CO, O₃, and SO₂. The DA of NO₂ is excluded in the
772 current study, the reason for which is discussed in the text.



773

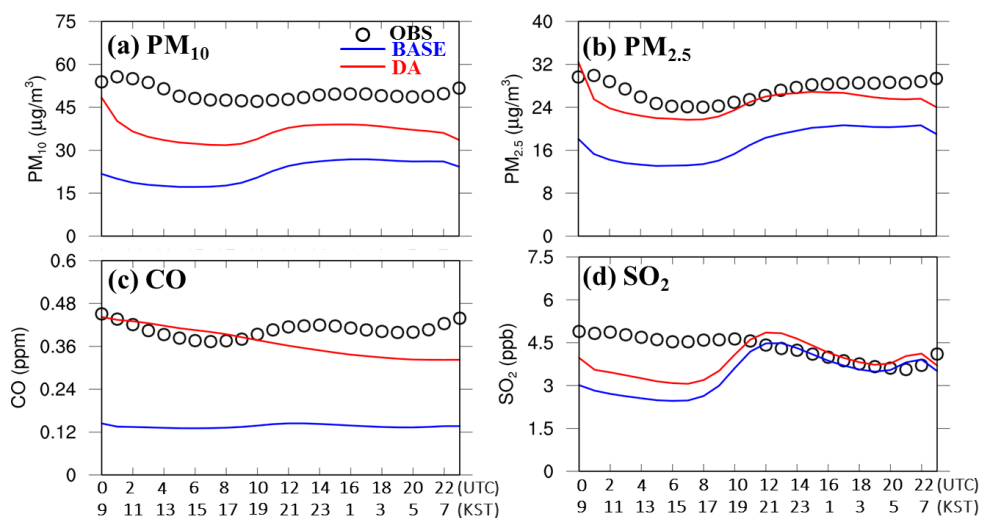
■ SULFATE ■ NITRATE ■ AMMONIUM ■ OA ■ EC ■ OTHERS

774 **Figure 4.** Average PM_{2.5} composition (a) observed at the super-site stations and (b) simulated
775 by the CMAQ model during the KORUS-AQ campaign. The averaged PM_{2.5} measured from the
776 super-sites and calculated from the CMAQ model simulations over the period of the
777 KORUS-AQ campaign are 28 µg/m³ and 19.9 µg/m³, respectively. The mass of organic
778 aerosols (OAs) was calculated by multiplying organic carbon mass by 1.6.



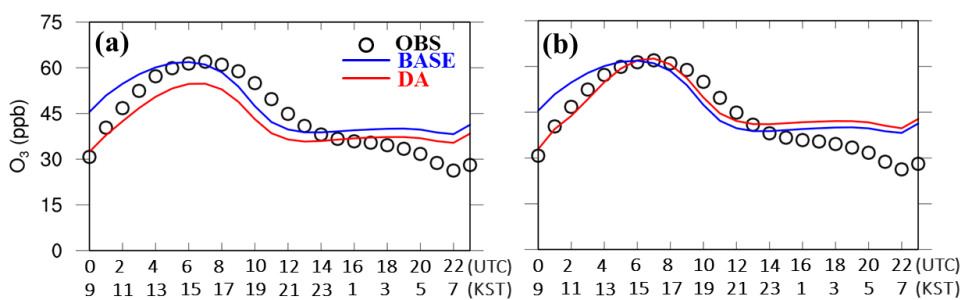
779

780 **Figure 5.** Time-series plots of hourly (a) PM_{10} , (b) $\text{PM}_{2.5}$, (c) CO, (d) SO_2 , and (e) O_3
781 concentrations at 264 Air Korea stations. Black open circles (OBS) represent the observed
782 concentrations. Blue and red lines show the results simulated from the BASE RUN and DA
783 RUN over South Korea, respectively.



784

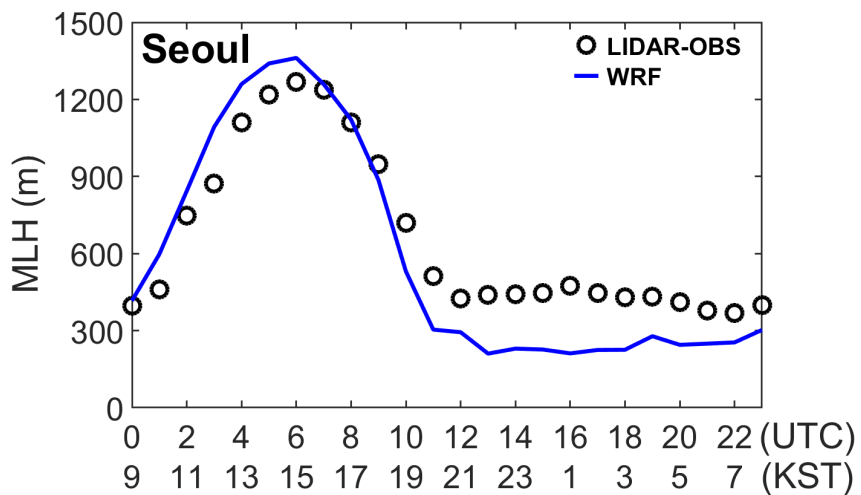
785 **Figure 6.** Aggregated average concentrations of (a) PM_{10} , (b) $\text{PM}_{2.5}$, (c) CO , and (d) SO_2 at
786 264 Air Korea stations over the KORUS-AQ campaign period. Open black circles denote the
787 observations obtained from 264 Air Korea stations in South Korea. Blue and red lines
788 represent the predicted concentrations from the BASE RUN and DA RUN, respectively. The
789 DA was conducted at 00:00 UTC every day throughout the KORUS-AQ campaign period.



790

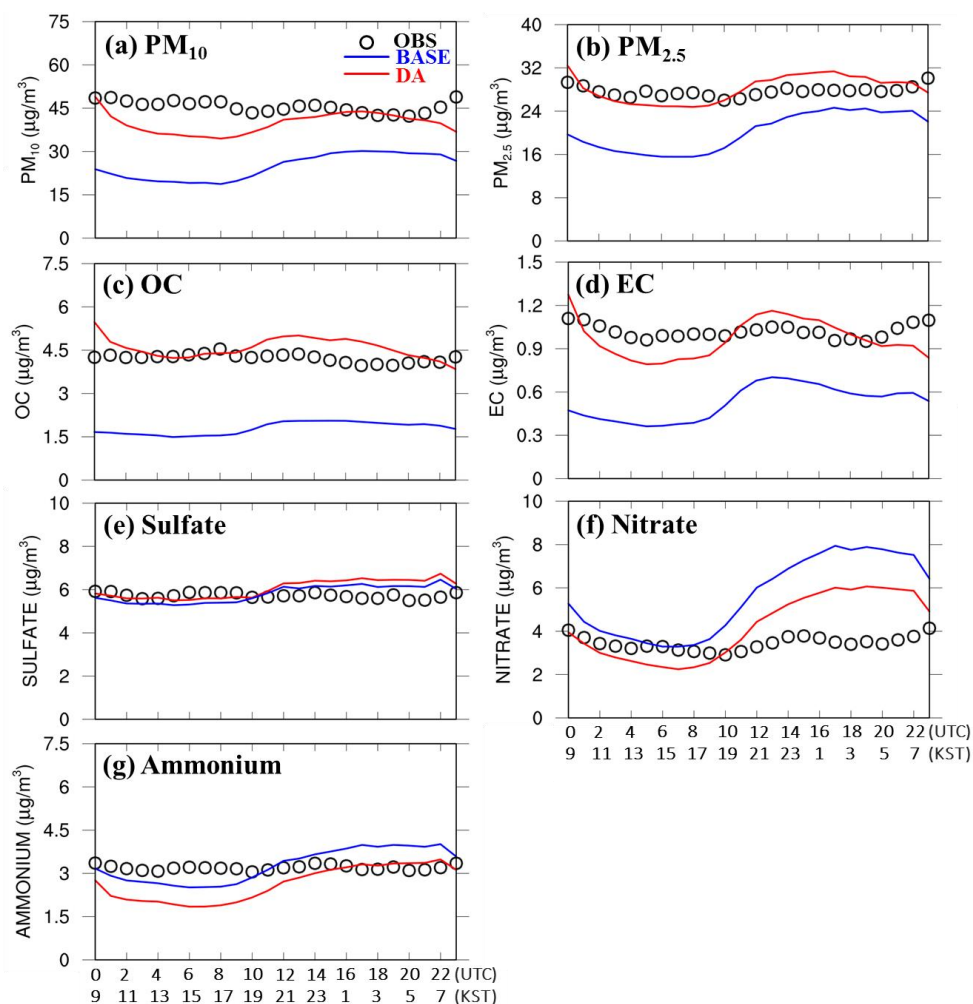
791 **Figure 7.** Comparison of CMAQ-simulated O₃ mixing ratios (BASE RUN with blue lines
792 and DA RUN with red lines) with O₃ mixing ratios from Air Korea stations (open black
793 circles). DA RUN was carried out by assimilating CMAQ outputs with Air Korea
794 observations using (a) only O₃ mixing ratios and (b) both O₃ and NO₂ mixing ratios.

795



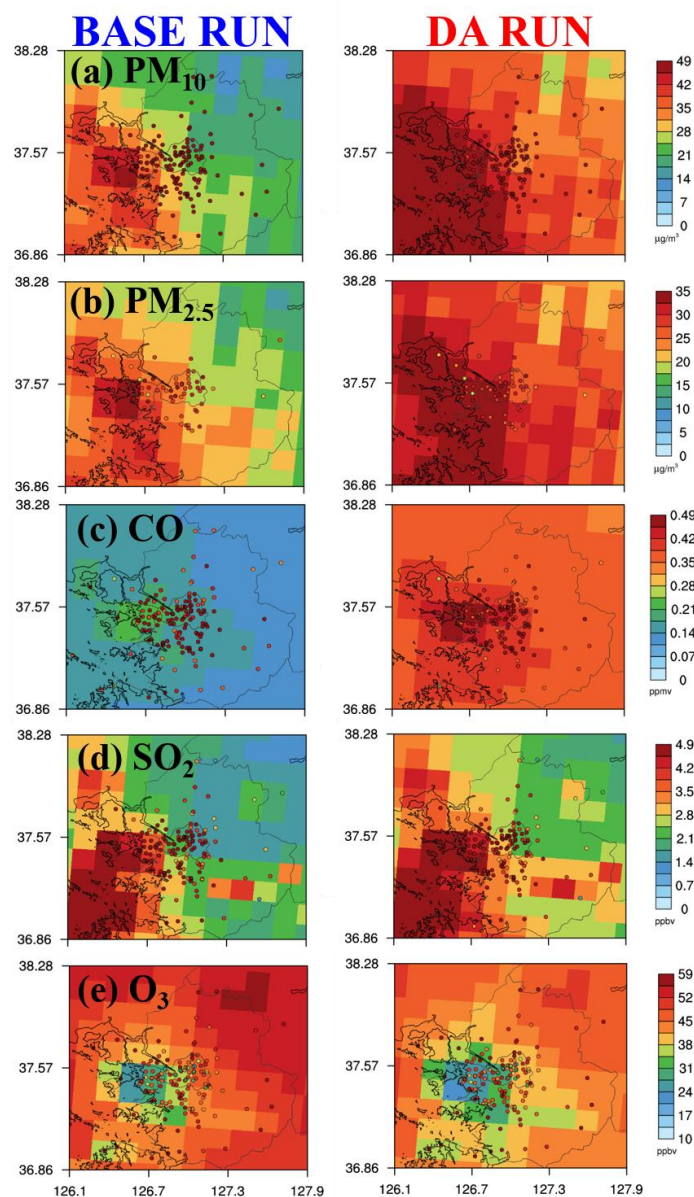
796

797 **Figure 8.** Comparison of WRF-simulated mixing layer height (MLH) (denoted by blue-
798 dashed line) with lidar-measured MLH (denoted by open black circles) at Seoul National
799 University (SNU) in Seoul. KST stands for Korean standard time.



800

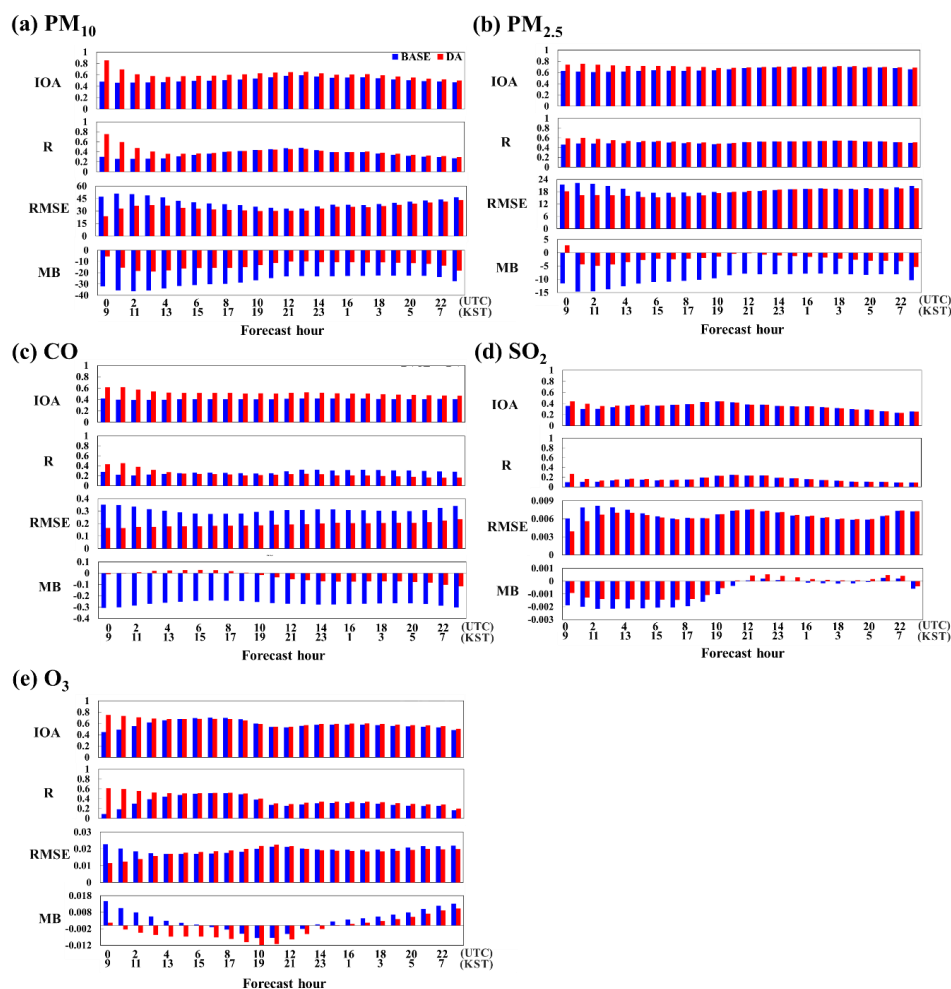
801 **Figure 9.** Aggregated average concentrations of (a) PM_{10} , (b) $PM_{2.5}$, (c) OC, (d) EC, (e)
802 sulfate, (f) nitrate, and (g) ammonium as predicted by CMAQ model during the period of the
803 KORUS-AQ campaign. The others are the same as those shown in Fig. 7, except for the fact
804 that the observation data used here were obtained from the seven super-site stations in South
805 Korea.



806

807 **Figure 10.** Spatial distributions of (a) PM₁₀, (b) PM_{2.5}, (c) CO, (d) SO₂, and (e) O₃ over Seoul
808 Metropolitan Area (SMA). The concentrations were averaged over the entire period of the
809 KORUS-AQ campaign. Colored circles represent the concentrations of the air pollutants
810 observed at the Air Korea stations in the SMA.

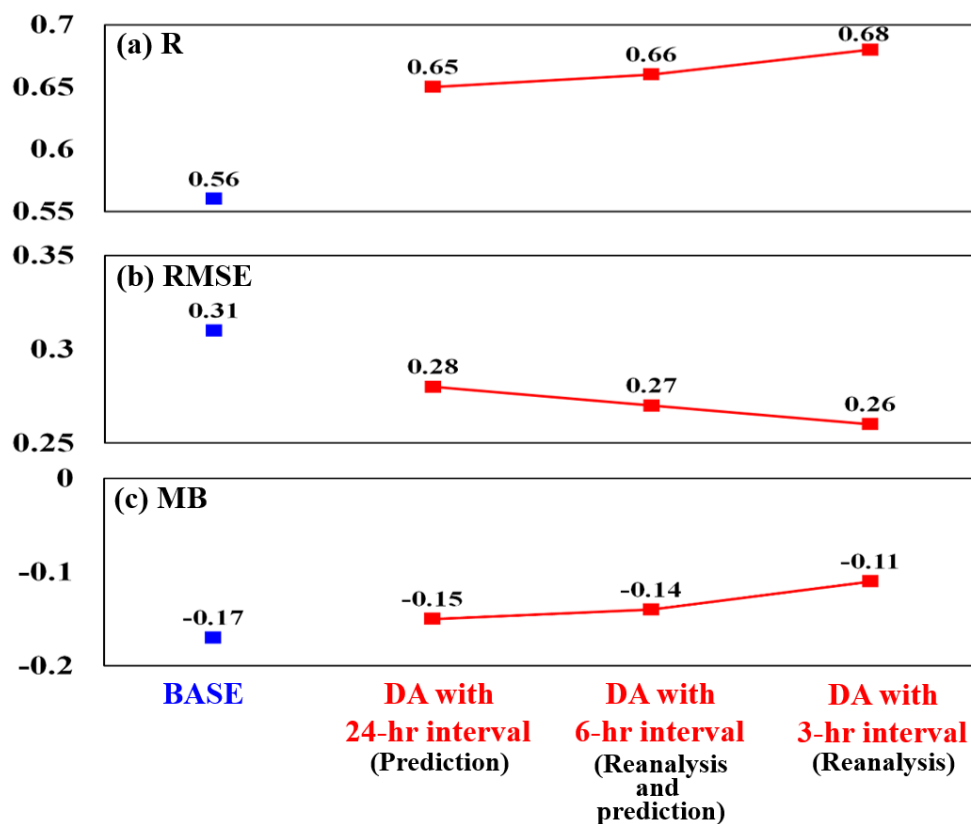
811



812

813 **Figure 11.** Time-series plots of four performance metrics (IOA, R, RMSE, and MB) for (a)
814 PM₁₀, (b) PM_{2.5}, (c) CO, (d) SO₂, and (e) O₃ forecasts. The DA was conducted at 00:00 UTC.
815 The units of RMSE and MB are $\mu\text{g}/\text{m}^3$ and ppmv for PM concentrations and for gaseous
816 species, respectively. The definitions of the four performance metrics are shown in Appendix
817 A.

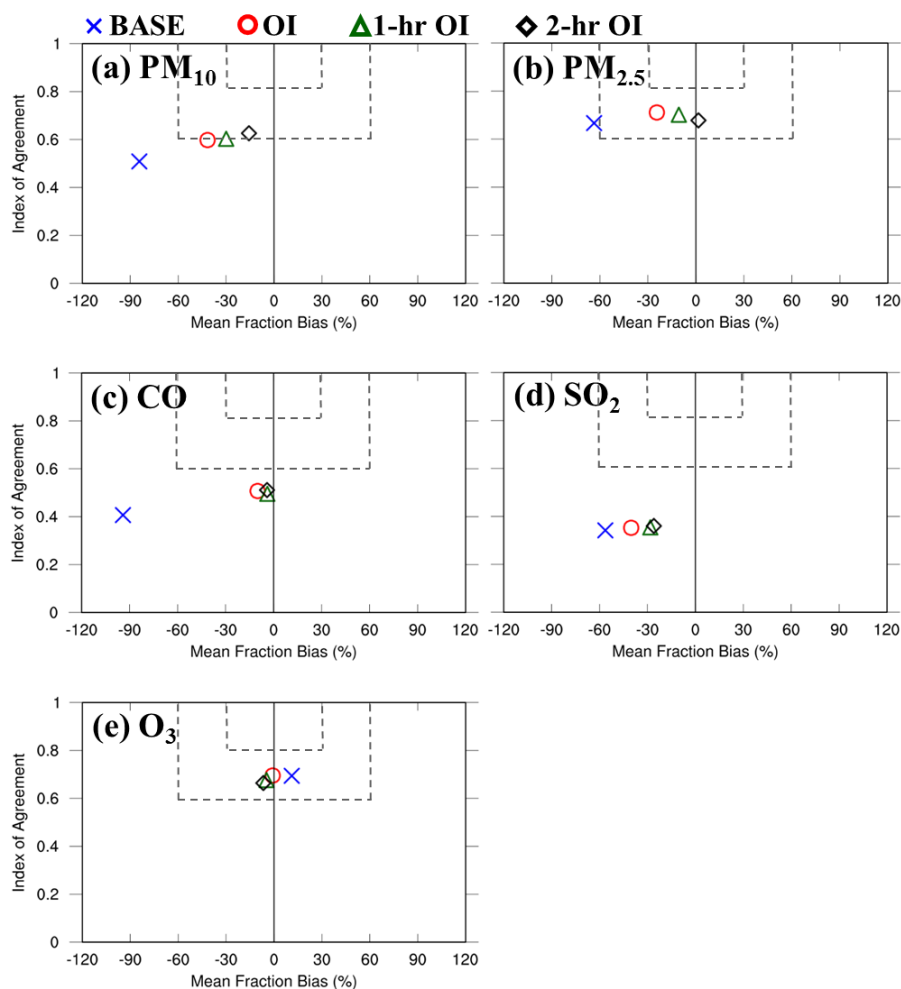
818



819

820 **Figure 12.** Variations of three performance metrics (R, RMSE, and MB) with time-intervals
821 of data assimilations. For these tests, the GOCI AODs were used in the DA to update the
822 initial conditions of the CMAQ model simulations. The results from the three CMAQ model
823 simulations were compared with AERONET AODs (“ground truth”). The two blue squares
824 represent the performances from the BASE RUNs and the red squares indicate the
825 performances from the DA RUNs. The three experiments were carried out with the
826 assimilation time-intervals of 24, 6, and 3 hours (hr), respectively. Here, the DA RUN with
827 the 24-hr time-interval is referred to as “air quality prediction”, and the DA RUNs with the 6-
828 hr and 3-hr time-interval are referred to as “air quality reanalysis”.

829



830

831 **Figure 13.** Soccer plot analyses for (a) PM₁₀, (b) PM_{2.5}, (c) CO, (d) SO₂, and (e) O₃. The
832 CMAQ-predicted concentrations were compared with the Air Korea observations. Blue
833 crosses, red circles, dark-green triangles, and black diamonds represent the performances
834 calculated from the BASE RUN, the DA RUNs with the OI system, the 1-hour (hr) OI system,
835 and the 2-hr OI system, respectively.



836 **Table 1.** Statistical metrics from BASE RUN and DA RUN with Air Korea observations over
 837 the entire period of the KORUS-AQ campaign.

	PM ₁₀		PM _{2.5}		CO		SO ₂		O ₃	
	BASE RUN	DA RUN	BASE RUN	DA RUN	BASE RUN	DA RUN	BASE RUN	DA RUN	BASE RUN	DA RUN
N	101852		65383		101764		101764		101836	
IOA	0.51	0.60	0.67	0.71	0.41	0.51	0.34	0.35	0.69	0.70
R	0.34	0.40	0.51	0.53	0.28	0.21	0.14	0.15	0.50	0.52
RMS E	40.8	34.87	19.2	17.83	0.31	0.19	0.0068	0.0066	0.020	0.02
MB	-27.2	-13.54	-9.9	-2.43	-0.27	-0.04	-0.0009	-0.0004	0.003	-0.0024
ME	30.1	24.20	15.3	13.48	0.27	0.15	0.004	0.0034	0.015	0.015
MNB	-50.0	-18.17	-30.1	5.32	-62.0	3.14	3.1	17.77	48.0	30.22
MNE	60.7	52.35	62.6	62.77	62.9	40.67	93.1	93.56	70.2	61.34
MFB	-84.3	-41.61	-63.6	-24.41	-94.1	-10.00	-56.4	-40.20	11.1	-0.82
MFE	91.1	62.32	81.6	60.01	94.9	39.49	91.4	82.91	40.7	40.64

838



839 **Table 2.** Statistical metrics from BASE RUN and DA RUN with Air Korea observations at
 840 00:00 UTC when the DA was conducted during the KORUS-AQ campaign.

	PM ₁₀		PM _{2.5}		CO		SO ₂		O ₃	
	BASE RUN	DA RUN	BASE RUN	DA RUN	BASE RUN	DA RUN	BASE RUN	DA RUN	BASE RUN	DA RUN
N	1057		695		1024		1007		1043	
IOA	0.48	0.86	0.63	0.74	0.41	0.62	0.36	0.44	0.45	0.75
R	0.30	0.75	0.46	0.59	0.28	0.43	0.097	0.27	0.09	0.61
RMS E	47.2	23.92	21.5	18.21	0.35	0.16	0.0061	0.0039	0.023	0.012
MB	-32.2	-5.46	-11.5	2.80	-0.31	-0.01	-0.0019	-0.0009	0.015	0.002
ME	34.5	16.03	17.2	13.25	0.31	0.12	0.0039	0.0023	0.018	0.009
MNB	-54.9	-0.53	-33.2	26.17	-64.3	9.69	-20.1	7.35	100.4	27.45
MNE	64.0	36.07	63.1	59.77	64.8	30.69	86.7	55.27	107.8	43.81
MFB	-92.8	-13.38	-67.3	0.56	-98.7	1.81	-75.9	-17.39	43.7	12.16
MFE	98.8	38.41	84.3	48.30	99.1	27.14	99.9	56.23	52.9	31.53

841